Unravelling the Interaction of Water-in-Oil Emulsion Droplets via Molecular Simulations and Surface Force Measurements

Xiaoyu Sun[†], Diling Yang [†], Hao Zhang[†], Hongbo Zeng[,†], Tian Tang[*,‡]*

[†]Department of Chemical and Materials Engineering, University of Alberta, Edmonton, AB T6G 1H9, Canada

[‡]Department of Mechanical Engineering, University of Alberta, Edmonton, AB T6G 1H9, Canada

** Corresponding authors:*

E-mail: hongbo.zeng@ualberta.ca (H.Z.); Phone: +1-780-492-1044;

E-mail: tian.tang@ualberta.ca (T.T.); Phone: +1-780-492-5467.

ABSTRACT

Water-in-oil emulsions widely exist in various chemical and petroleum engineering processes, and their stabilization and destabilization behaviors have attracted much attention. In this work, molecular dynamic (MD) simulations were conducted on the water-in-oil emulsion droplets with the presence of surface-active components, including a polycyclic aromatic compound (VO-79) and non-ionic surfactants: $PEO_5PPO_{10}PEO_5$ triblock copolymer and Brij-93. At the surface of water droplets, films were formed by the adsorbate molecules which redistributed during the approaching of the droplets. The redistribution of $PEO_5PPO_{10}PEO_5$ was more pronounced than Brij-93 and VO-79, which contributed to lower repulsion during coalescence. Also, the interaction forces during droplet coalescence were measured using atomic force microscopy (AFM). Jump-in phenomenon and coalescence were observed for systems with VO-79, Brij-93 and low concentration of Pluronic P123. The critical force before jump-in was lowest for low concentration of Pluronic P123, consistent with the MD results. Adhesion was measured when separating water droplets with high concentration of Pluronic P123. By correlating theoretical simulations and experimental force measurements, this work improves the fundamental understanding on the interaction behaviors of water droplets in oil medium in the presence of interface-active species and provides atomic level insights into the stabilization and destabilization mechanisms of water-in-oil emulsion.

1. INTRODUCTION

Water-in-oil emulsions are widely present in many environmental and industrial processes.[1–9] It is known that water droplets dispersed in an immiscible liquid (*e.g.*, oil) are thermodynamically unstable and tend to coalesce.[10,11] On the other hand, interfacial-active materials could adsorb at the oil/water interface, making the water droplets kinetically stable.[12,13] A stable emulsion is desirable in many applications, such as in cosmetics, pharmaceutical, food industries and biological applications.[14,15] While in petroleum industry, the presence of water-in-oil emulsion could reduce the quality of oil products and also cause severe technical problems such as corrosion and fouling.[16]

By investigating water droplets with the adsorption of various interfacial-active materials, the stability of emulsified droplets can be understood and manipulated. For example, polycyclic aromatic compounds (PACs) such as asphaltenes in natural crude oil are generally accepted as the main contributors to stabilize the unwanted water-in-crude-oil emulsion.[10] Using drop probe atomic force microscopy (AFM), the interaction forces between two micrometer-size water droplets stabilized by PACs in toluene, heptane and heptol (mixtures of toluene and heptane) were measured.[16] The water droplets underwent repulsive force during approaching due to the steric repulsion between interfacially adsorbed PACs films.[16] Adhesion between the droplets was found during their separation, which was caused by the interpenetration and aggregation of PACs at the oil/water interfaces.[16] The strength of adhesion increased with increasing PAC concentration up to a threshold and then significantly decreased with further increase of PAC concentration.[16] The water-in-crude-oil emulsion stabilized by interfacial-active components can be destabilized by adding chemical demulsifiers such as non-ionic surfactants or polymers. A previous work reported that PAC-stabilized water-in-toluene emulsion could be destabilized with the addition of PEO-

PPO copolymers as demulsifiers.[17] The amount of water resolved in the bottle test reached its maximum of ~85% when 2.3 ppm of PEO-PPO copolymers were applied.[17] With lower than 0.1 ppm of the demulsifiers, the water could not be separated from the toluene; and the resolved water decreased with further increase of PEO-PPO copolymers concentration from 2.3 ppm to 288.4 ppm.[17] By adding only PEO-PPO copolymers to the emulsion without PACs, the amount of resolved water was 100% when the PEO-PPO concentration was 2.3 ppm.[17] Similar to the systems with a mixture of demulsifiers and PACs, the water resolved in systems with only demulsifiers also decreased as the PEO-PPO concentration increased from 2.3 ppm to 230.7 ppm.[17] The previous results indicated that a suitable dosage of polymer demulsifier could facilitate the coalescence and demulsification of water-in-oil droplets with protective interfacial PACs films, however overdosage of the polymer could stabilize the emulsion drops.

Much progress has been achieved in experimental investigation on water droplets coalescence, which has also encountered some challenges, such as the difficulty to capture the rapid coalescence phenomenon[18] or nanometer-size droplets.[19] Molecular dynamics (MD) simulations have been carried out to provide molecular-level images on water droplet coalescence.[4,20–22] Jian *et al.* used MD simulations to study the adsorption of PACs on water droplets and its effect on water droplet coalescence.[23,24] At low concentration, the adsorption of PACs on the water droplets was incomplete, where the dispersed PAC molecules acted as a barrier to prevent droplets coalescence.[23,24] Evident adsorption of PACs was observed when their concentration was sufficiently high.[23,24] A protective film of PACs was formed at the surface of water droplets which prevented coalescence.[23,24] Pak *et al.* performed MD simulations and potential of mean force (PMF) calculations on the coalescence of water droplets uncoated[25] and coated by organic compounds (benzoic acid, heptanoic acid, and pimelic acid).[26] The free energy profiles suggested that the

coalescence was spontaneous or energetically preferable for water droplets with and without coated materials.[25,26] These free energy calculations were carried out on water droplets in the atmosphere.[25,26] Sicard *et al.* investigated the water droplets in organic solvent (decane) with interfacially adsorbed nanoparticles by using dissipative particle dynamics.[15] The free energy profiles indicated that the nanoparticles reduced the fragmentation free energy during the breakup of water nanodroplets, facilitating emulsification.[15] Despite these few works, quantitative analysis on the stabilization of water-in-oil emulsion by surface-active components and their destabilization by demulsifiers is scarce and still in demand. Systematic investigation from both simulations and experiments will benefit the mechanistic understanding on the interaction of water-in-oil emulsion droplets.

In this work, MD simulations were performed on water droplets in oil (represented by toluene) with three different interfacial-active components: a model PAC, violenthrane-79 (VO-79), and two non-ionic surfactants, PEO-PPO-PEO triblock copolymer and Brij-93. PACs, including VO-79, have been considered as a model stabilizer for water droplets in oil phase.[23,24] PEO-PPO-PEO triblock copolymers have been extensively used as demulsifiers. A model PEO-PPO-PEO triblock copolymer, $PEO_5PPO_{10}PEO_5$, was employed and compared with another low molecular weight non-ionic surfactant Brij-93, which has also been studied as a demulsifier.[27,28] The coalescence of two adsorbate-coated water droplets was simulated, and the free energy profiles and interaction forces during the coalescence were calculated. In addition, the interaction forces between water droplets were measured using the drop probe AFM technique and correlated to the MD simulations. Bridging the gap between simulations and experiments, this study aims to provide atomic level understanding on the coalescence of water-in-oil emulsion droplets. This work provides useful

insights into emulsification and demulsification problems, and the methodologies could be readily extended to similar systems involving droplet interactions.

2. METHODS

2.1 Simulation models and systems.

Three types of interfacial-active molecules were used as adsorbates at the interface between water and oil (represented by toluene). As shown in Fig. 1a, violenthrane-79 (VO-79, $C_{50}H_{48}O_4$, molecular weight MW: 712 g/mol) is a PAC with a PA core (marked in dashed blue rectangle) and two peripheral chains. A hypothetical model PEO-PPO-PEO copolymer (Fig. 1b), $PEO_5PPO_{10}PEO_5$ (MW: 1039 g/mol), was built and applied in the simulations. Hydrophilic PEO groups are marked in dashed blue rectangles as shown in Fig. 1b. Another non-ionic surfactant simulated was polyethylene glycol oleyl ether Brij-93 ($C_{22}H_{44}O_3$, MW: 357 g/mol), as shown in Fig. 1c where the hydrophilic group is highlighted. Force field parameters of the three molecules were validated in our previous works and directly adopted [29–31]. Briefly, chemical structures for the non-ionic surfactants were drawn in ChemDraw Prime 16.0. The geometry and force field parameters were optimized using Gaussian 16 [32] at the B3LYP [33]/6-31G + (d,p) level, with partial charge calculated with CHELPG (CHarges from ELectrostatic Potentials using a Grid based method) [34]. Automated Topology Builder (ATB) [35] was used to further optimize the obtained geometry and generate the topology compatible with GROMOS parameter sets [36].

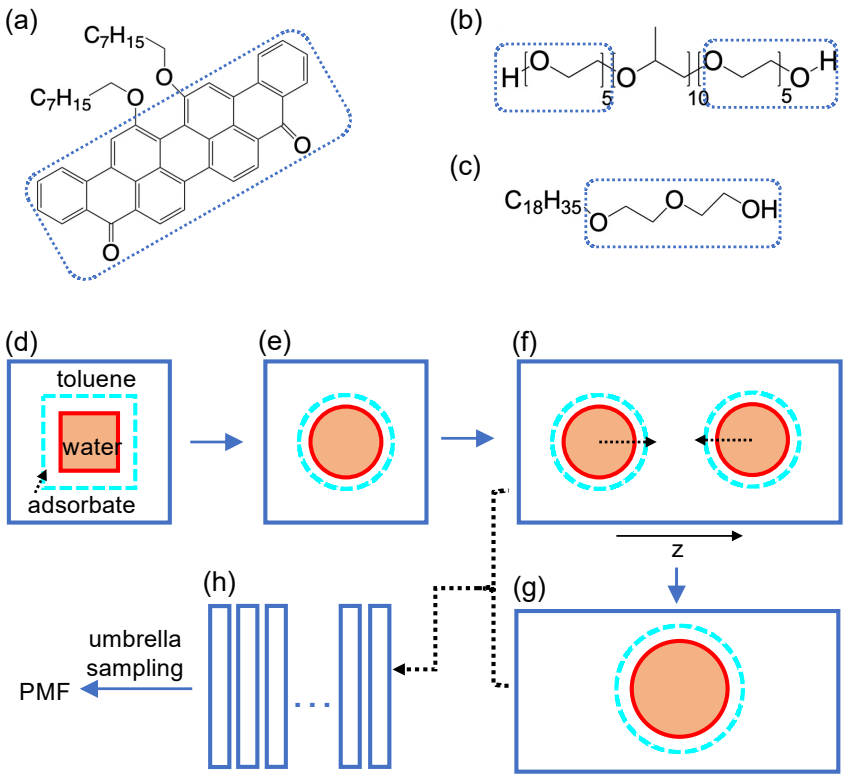

Figure 1. Molecular structure for (a) VO-79, (b) $PEO_5PPO_{10}PEO_5$, and (c) Brij-93; (d-h) schematics of simulation procedures.

Details of the simulated systems are shown in Table 1. Sys. A0 represented the control system with no adsorbates. Each of the other systems contained a single type of adsorbates, and was named with V, P and B representing VO-79, $PEO_5PPO_{10}PEO_5$ and Brij-93, respectively. The adsorbate concentration was lower in sys. V1, P1, and B1 than that in sys. V2, P2, and B2, respectively. Each system had two water droplets that were built by duplicating a system with a single water droplet. The systems with a single water droplet were named with "-S" appended to the name of their corresponding system with two water droplets. There were 96 VO-79 molecules in sys. V1-S, 34 $PEO_5PPO_{10}PEO_5$ molecules in sys. P1-S, and 77 Brij-93 in sys. B1-S. These numbers of VO-79 molecules were chosen to obtain a similar surface coverage of the water droplet (approximately

46-47%) in V1-S, P1-S and B1-S, as shown in Supporting Information (SI) section SI1. There were 196 VO-79 molecules in sys. V2-S, so that the mass concentration of VO-79 in sys. V2 was approximately twice that in sys. V1. Similarly, the mass concentration of $PEO_5PPO_{10}PEO_5$ in sys. P2 was about twice the concentration of $PEO_5PPO_{10}PEO_5$ in sys. P1. The mass concentration of Brij-93 in sys. B2 was comparable to the mass concentration of $PEO_5PPO_{10}PEO_5$ in sys. P2.

Table 1. System details. Surface coverage fraction was obtained from the equilibrated system containing a single water droplet.

sys.	adsorbate	mass concentration of adsorbate (ppm)	single water droplet		
			sys.	# of adsorbates	surfaces coverage fraction
A0	-	-	A0-S	-	-
V1	VO-79	44,789	V1-S	96	47%
P1	$PEO_5PPO_{10}PEO_5$	22,568	P1-S	34	47%
B1	Brij-93	17,553	B1-S	77	46%
V2	VO-79	97,558	V2-S	196	61%
P2	$PEO_5PPO_{10}PEO_5$	46,027	P2-S	66	72%
B2	Brij-93	45,807	B2-S	192	78%

2.2 Simulation details.

All simulations were performed using the GROMACS package [37–39] (version 5.0.7) with GROMOS force field parameter set 54A7 [40]. There were three phases in the simulations. The first phase was the simulation for a single water droplet in sys. A0-S, V1-S, P1-S, B1-S, V2-S, P2-S, or B2-S, as shown in Fig. 1d (initial configuration) and Fig. 1e (final configuration). The second phase was steered MD (SMD) simulation where two water droplets were pulled towards each other till coalescence, as shown in Fig. 1f (initial configuration) and Fig. 1g (final configuration). The

third phase was umbrella sampling (US) simulations to generate the PMF between the two water droplets, as shown in Fig. 1h.

In each single droplet simulation (Fig. 1d), a water box with dimension of 5×5×5 nm^3 was constructed and centered in a 14×14×14 nm^3 box. For the control system with no adsorbates, the water box was then solvated by toluene molecules. For systems with adsorbates, the adsorbate molecules were placed in arrays on the six sides of the water box (Fig. 1d) before filling the larger box with toluene molecules. Each system with a single water droplet underwent energy minimization (EM) using steepest descent method, NVT equilibration, and production simulation in NPT ensemble. NVT equilibration was performed for 100 ps with position-restraints, where harmonic potential of force constant 1000 kJ/(mol·nm^2) was applied on the non-hydrogen atoms in the adsorbate molecules. With the restraint removed, production simulation was carried out at 300 K and 1 bar. Pressure coupling was applied by using Parrinello-Rahman [41] barostat with time constant (τ_p) of 1.0 ps. Velocity rescaling thermostat with a time constant (τ_T) of 0.1 ps was used for temperature coupling. LINCS [42] algorithm, Particle Mesh Ewald method for full electrostatics [43], and periodic boundary conditions in all directions (x, y, z) were applied. Twin-range cut-offs were used for van der Waals and electrostatic interactions with a cut-off of 1.4 nm. All simulations had a time step of 2 fs, and the simulation time for each system was 60 ns. After equilibrium, a single water droplet was formed and surrounded by the adsorbate molecules, as shown in Fig. 1e.

SMD simulations were performed to expedite the coalescence of two water droplets by applying external force on their centers of mass (COMs). To obtain two water droplets, the configuration of an equilibrated single droplet (Fig. 1e) was duplicated along z direction, forming a simulation box approximately 14×14×28 nm^3 in dimension (Fig. 1f). After EM and NVT equilibration following the same procedure as described above, SMD was carried out. The simulation parameters in SMD

were similar to those in the production MD in phase 1, except that pressure coupling was removed and NVT ensemble was used in the SMD [25,26]. Each droplet contained a large cluster of water molecules where any water molecule had at least one neighboring water molecule within 0.35 nm [44]. The atom indices in this cluster were used to define the COM of the droplet, and a harmonic potential was applied on the two COMs with a spring constant of 1000 kJ/(mol·nm^2). It is worth noting that after EM and NVT equilibration just before SMD, the COMs of two water droplets may not be aligned exactly along z direction. The reaction coordination (ζ) was selected as the distance between the two COMs, *i.e.*, along the head-on direction. COMs of both water droplets were pulled closer at a net pull rate of 0.01 nm/ps. Such rate was selected based on the following considerations. Firstly, in Lemkul and Bevan's work [45] of dissociating two peptides, the trajectory and force profile resulted from the pull rate of 0.01 nm/ps was almost identical to those resulted from the pull rate of 0.005 and 0.001 nm/ps. Secondly, the primary aim of SMD here was to generate the trajectory of water droplet coalescence, while more quantitative analysis on PMF was performed by US. The total pull time was 1.4 ns and a total of 140 configurations were obtained from every 10 ps of the 1.4 ns simulation. Since the COM distance in the initial configuration (Fig. 1f) was 14 nm, the two droplets merged into a single droplet (Fig. 1g) at the end of the SMD, with the final COM separation of approximately 0 nm.

US was carried out to compute the PMF along the reaction coordinate (ζ). The range of ζ was selected to sample from the maximum COM separation (~14 nm) to the separation where the droplets merged. A total of 43-50 US windows were used, in order to render good overlap (SI section SI2) between the probability distributions from neighboring US simulations [45,46]. During each US simulation, an external biasing potential with spring constant of 2000 kJ/(mol·nm^2) was applied on the COMs of the two droplets, at the corresponding US window. After a brief NVT

equilibration, the US simulation was run for 2 ns using an SMD at zero pull rate. Data collected from US was analyzed by the weighted histogram analysis method (WHAM) [45,47] to generate the unbiased PMF as a function of the reaction coordinate (ζ).

2.3 Drop probe atomic force microscope (AFM).

The interaction forces between two water droplets in different organic solutions were investigated using a drop probe AFM technique, and the schematic of a typical experimental setup is shown in Fig. 2a. Three types of interfacial-active materials, VO-79, Pluronic P123 and Brij-93 (as received from Sigma-Aldrich), were dispersed in toluene solutions at 1 ppm and 1000 ppm for VO-79, 0.1 ppm and 5 ppm for Pluronic P123, and 1 ppm and 1000 ppm for Brij-93. Pluronic P123 has a molecular structure of $(PEO)_{20}(PPO)_{70}(PEO)_{20}$, where its PEO-PPO-PEO triblock architecture and high EO content (30 wt.%) shared similarities with the hypothetical model $PEO_5PPO_{10}PEO_5$ in our simulations.

In a typical experiment, the glass substrate of AFM fluid cell was pre-hydrophobized by immersing it in an octadecyltrichlorosilane (OTS) solution in toluene. A water contact angle of ~90° was obtained to facilitate the lifting of water droplet. Water droplets were generated and injected into the AFM fluid cell containing a desired concentration of adsorbates in toluene using a custom-made ultrasharp glass pipet. To prepare a water droplet probe, a custom-made tipless rectangular silicon AFM cantilever ended with a circular gold patch was first pre-treated by immersing it in a 11-mercapto-1-undecanol solution in ethanol. After achieving a water contact angle of ~40°, the cantilever was used to pick up a water droplet of suitable size in the AFM fluid cell. The water droplet probe was positioned above another droplet of similar size on the substrate for the force measurement. The spring constant of the cantilever was calibrated using Hutter's method before anchoring the water drop [48]. To minimize the hydrodynamic effect on the force

measurements, the driving velocity of the upper water droplet was set as 1 μm/s. The interaction forces were determined via Hooke's law by detecting the deflection of the cantilever using the AFM software. During the force measurements, water droplets were aged in the adsorbate solutions for a certain time (viz., 5 min unless otherwise specified), and the maximum load was set as 5 nN in all the measurements. The measurement for a control system with bare water droplets in pure toluene is shown in Fig. 2b.

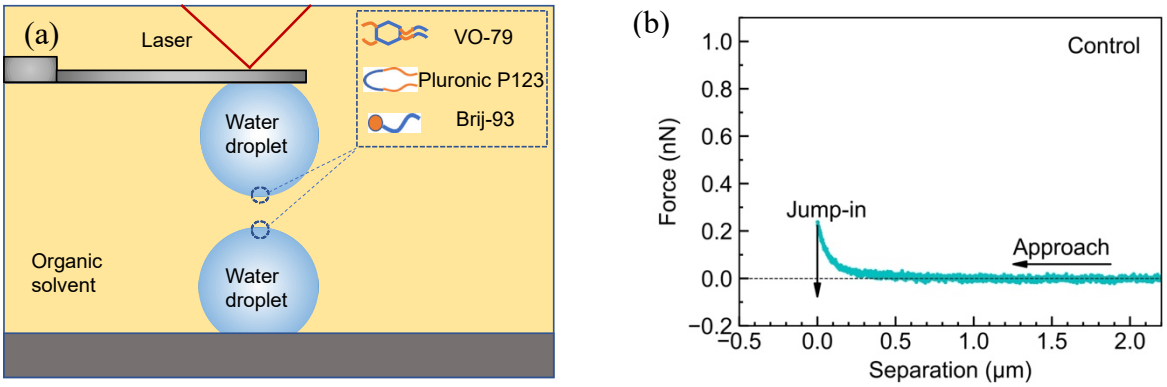

Figure 2. (a) Schematic of experimental setup for measuring the interaction forces between two water droplets in an organic solvent using the droplet probe AFM technique; (b) interaction force profile measured between two bare water droplets in pure toluene (control system).

3. RESULTS AND DISCUSSION

3.1 Adsorbate film on water droplet.

Fig. 3a shows the final configurations of MD simulations for systems containing a single water droplet. Without adsorbates (sys. A0-S), a sphere-like water droplet was formed in toluene. As shown in SI section SI1, the diameter for a droplet containing 4074 water molecules was estimated to be D_p = 6.156 nm (radius R_p = 3.078 nm). For sys. V1-S, most of the VO-79 molecules (90 out

of 96) were adsorbed on the water droplet, forming a patchy interfacial film. In sys. P1-S and sys. B1-S, all the 34 $PEO_5PPO_{10}PEO_5$ and 77 Brij-93 molecules were adsorbed on the water droplets, resulting in surface coverage fraction comparable to that in sys. V1-S as shown in Table 1.

The thickness of the interfacial films was analyzed by the radial distribution function (RDF) of all atoms in the adsorbate molecules with respect to the COM of the water droplet. The RDFs were averaged over the last 5 ns of simulation, as shown in Fig. 3b for sys. V1-S, P1-S and B1-S. The distance (d) from the COM of water droplet was normalized by the droplet radius (R_p) on the horizontal axis of the plot. For each system in Fig. 3b, a single pronounced peak was located at d/R_p around 1.0-1.2, indicating the formation of a film on the surface of the water droplet. The thickness of the adsorbate film was represented by the width of the RDF peak in Fig. 3b, which from the thickest to thinnest followed: sys. V1 > sys. P1 > sys. B1.

RDFs for different atom groups in the adsorbates with respect to the COM of water droplet are shown in Fig. 3c for sys. V1-S, P1-S and B1-S. The location and width of the RDF peaks were summarized in SI section SI3. The group of atoms located closer to the water phase (smaller d/R_p at the RDF peak) was named group 1 (g1) for each type of adsorbates, which corresponded to the PA core in VO-79 and hydrophilic groups in $PEO_5PPO_{10}PEO_5$ and Brij-93 as marked in Fig. 1a-c. The other atom group, *i.e.*, side chains in VO-79 and hydrophobic groups in $PEO_5PPO_{10}PEO_5$ and Brij-93, was found further from the droplet COM (larger d/R_p at the RDF peak) and was named group 2 (g2). For VO-79, the oxygen functionality in the PA core formed hydrogen bonds with the water molecules [49]. The two non-ionic surfactants had amphiphilic feature and the hydrophilic groups interact more strongly with the water molecules. Comparing group 1 in sys. V1-S, P1-S and B1-S, the location of the RDF peak from furthest to nearest was ranked as: sys. V1-S > sys. P1-S slightly > sys. B1-S, as shown in SI section SI3. This result indicated that the hydrophilic

groups in $PEO_5PPO_{10}PEO_5$ and Brij-93 were closer to the water phase than the PA core group in VO-79. The same trend was found for the distribution of group 2 around the droplet COM; both were also consistent with the ranking of film thickness.

For systems with higher concentration of adsorbates (sys. V2-S, P2-S, B2-S), as shown in Fig. 3a, protective films were also formed at the droplet surface. In Fig. 3d, a single peak was observed in each RDF curve, and the width of the RDF peak representing film thickness was larger than the corresponding systems with less adsorbates (SI section SI3). Comparing different adsorbates, the film thickness followed the ranking of sys. V2-S > P2-S > B2-S. Observations in Fig. 3e for different atom groups were similar to those in Fig. 3c.

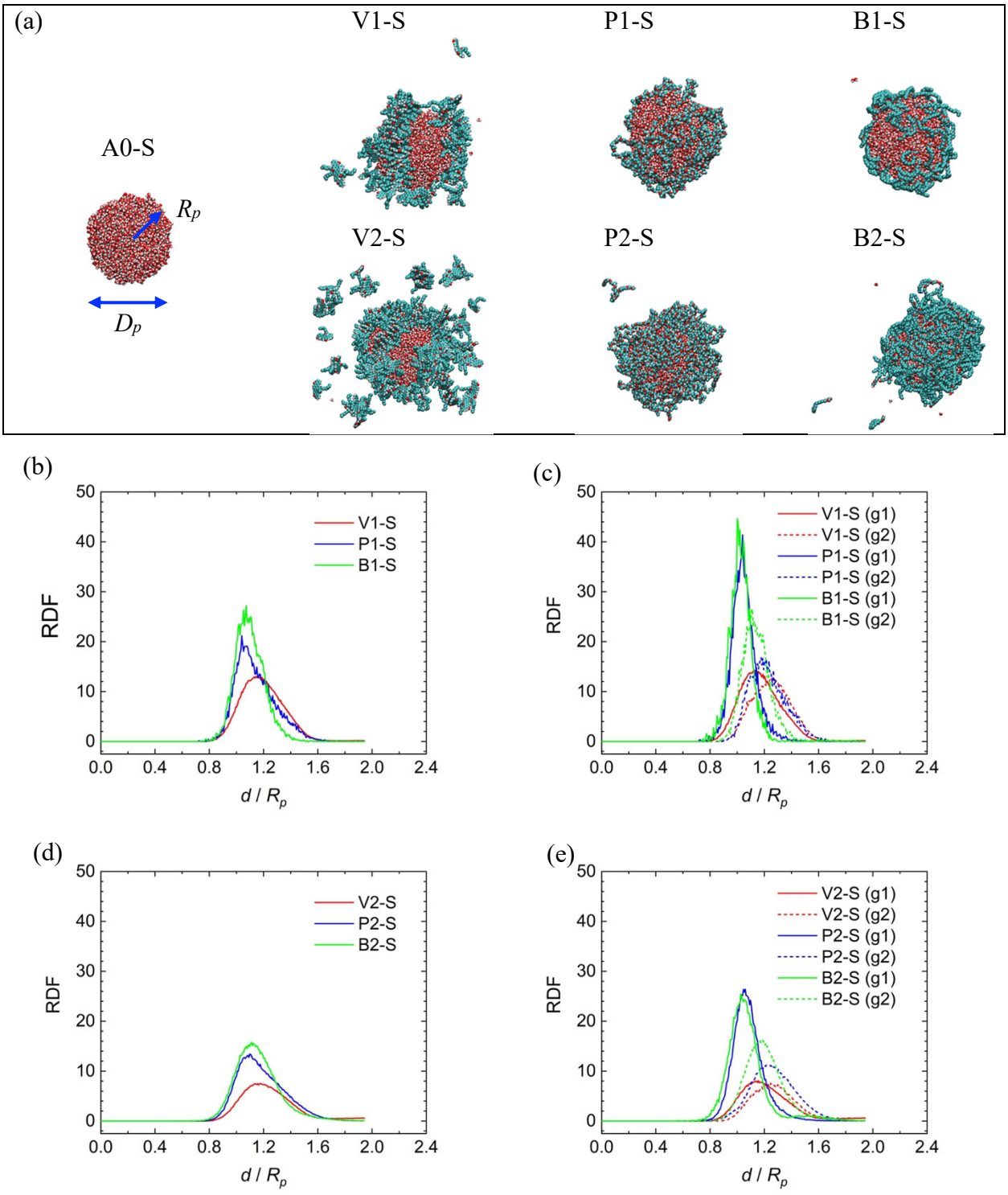

Figure 3. (a) Snapshots of final configurations for all systems containing a single water droplet (atoms were shown as van der Waals spheres, oxygen: red; hydrogen: grey; carbon: cyan; toluene molecules eliminated for clarity). RDF for all atoms in adsorbate molecules with respect to COM

of water droplet: (b) sys. V1-S, P1-S, B1-S; and (d) sys. V2-S, P2-S, B2-S. RDF for atoms in PA core (g1) and side chains (g2) of VO-79, in hydrophilic (g1) and hydrophobic (g2) groups of $PEO_5PPO_{10}PEO_5$ and Brij-93, with respect to COM of water droplet: (c) sys. V1-S, P1-S, B1-S; and (e) sys. V2-S, P2-S, B2-S.

3.2 Coalescence of water droplets in SMD.

During the SMD, two water droplets were pulled along the reaction coordinate (ζ), *i.e.*, their COM separation. The snapshots for 0 ns, 0.7 ns, 0.8 ns, 0.9 ns, and 1.0 ns in SMD are shown in Fig. 4a for sys. A0, V1, P1, and B1 (from left to right). Additional snapshots, 1.1-1.4 ns for sys. A0, V1, P1 and B1, and 0-1.4 ns for sys. V2, P2, and B2, are shown in SI section SI4.

As shown in Fig. 4a, at $t = 0$ ns, ζ was approximately 14 nm (half of box length in z direction). With constant pulling rate of 0.01 nm/ps, ζ at 0.7 ns was around 7 nm, where the two droplets were in proximity of each other. For sys. A0, water molecules from the two droplets started to contact at 0.8 ns and continued to merge at 0.9 ns and 1 ns. In sys. V1, as the water droplets approached each other, the adsorbed VO-79 molecules redistributed on the surface, leaving the droplets uncovered in the head-on direction. At 0.8-1.0 ns, the water droplets contacted each other and merged. As shown in SI section SI4, during 1.1-1.4 ns, a single spherical droplet formed due to coalescence, and VO-79 molecules initially from different droplets redistributed on the merged larger droplet. For sys. P1, the $PEO_5PPO_{10}PEO_5$ molecules also redistributed on the droplet surface from 0 to 0.7 ns and drainage of the $PEO_5PPO_{10}PEO_5$ film between the two droplets was observed. There was still a gap between the two droplets at 0.8 ns, coalescence initiated at 0.9 ns and continued at 1.0 ns. Redistribution of $PEO_5PPO_{10}PEO_5$ molecules was also observed on the merged droplet during 1.1-1.4 ns (SI section SI4). Observations in sys. B1 were similar, except

that the initiation of coalescence was delayed to 1 ns, with some Brij-93 molecules still interfering with droplet contact at 0.9 ns.

In Fig. 4b, the number of hydrogen bonds (H-bonds) between water molecules from the droplets in different cases is plotted against the reaction coordinate ζ (normalized by D_p). Four data points in each curve were highlighted, which corresponded to t = 0.7 ns, 0.8 ns, 0.9 ns and 1.0 ns in the SMD. For sys. A0 at t = 0.7 and 0.8 ns, the number of H-bonds were zero when the water droplets were close and about to make contact ($\zeta/D_p \sim$ 1.1-1.3). At t = 0.9 ns, the number of H-bonds were 393 and it increased dramatically to 1286 at t = 1.0 ns. Similar trend was observed for sys. V1. The number of H-bonds was zero before contact (t = 0.7 ns) and increased after coalescence began (t = 0.8 ns) and progressed (t = 0.9 and 1.0 ns). The curves sys. P1 and sys. B1 shared the same trend, but with a delayed increase in the number of H-bonds, consistent with the observations in Fig. 4a.

As shown in the snapshots for sys. V2 in SI sections SI4, many VO-79 molecules were dispersed in the toluene phase (0 ns). During the approaching of water droplets (0-0.7 ns), the dispersed molecules were gradually excluded from the space between the two droplets. Similar to sys. V1, the VO-79 molecules redistributed on the droplet surfaces, which left water molecules uncovered in the head-on direction (SI section SI4). H-bonds were formed after 0.8 ns when the droplets started to merge, as shown in Fig. 4c. For sys. P2 from 0-0.8 ns, the $PEO_5PPO_{10}PEO_5$ film became thinner and the $PEO_5PPO_{10}PEO_5$ molecules redistributed on the droplet surface (SI section SI4). However, the exposure of water surface after $PEO_5PPO_{10}PEO_5$ redistribution in sys. P2 was less apparent at 0.9 ns compared with sys. P1, due to the high surface coverage of $PEO_5PPO_{10}PEO_5$. Droplet coalescence started after 0.9 ns and H-bonds formed between them (Fig. 4c). Brij-93 in

sys. B2 formed a very uniform coating on the droplet surfaces (SI section SI4); and the merging of water droplets and formation of H-bonds initiated after 1.0 ns (Fig. 4c).

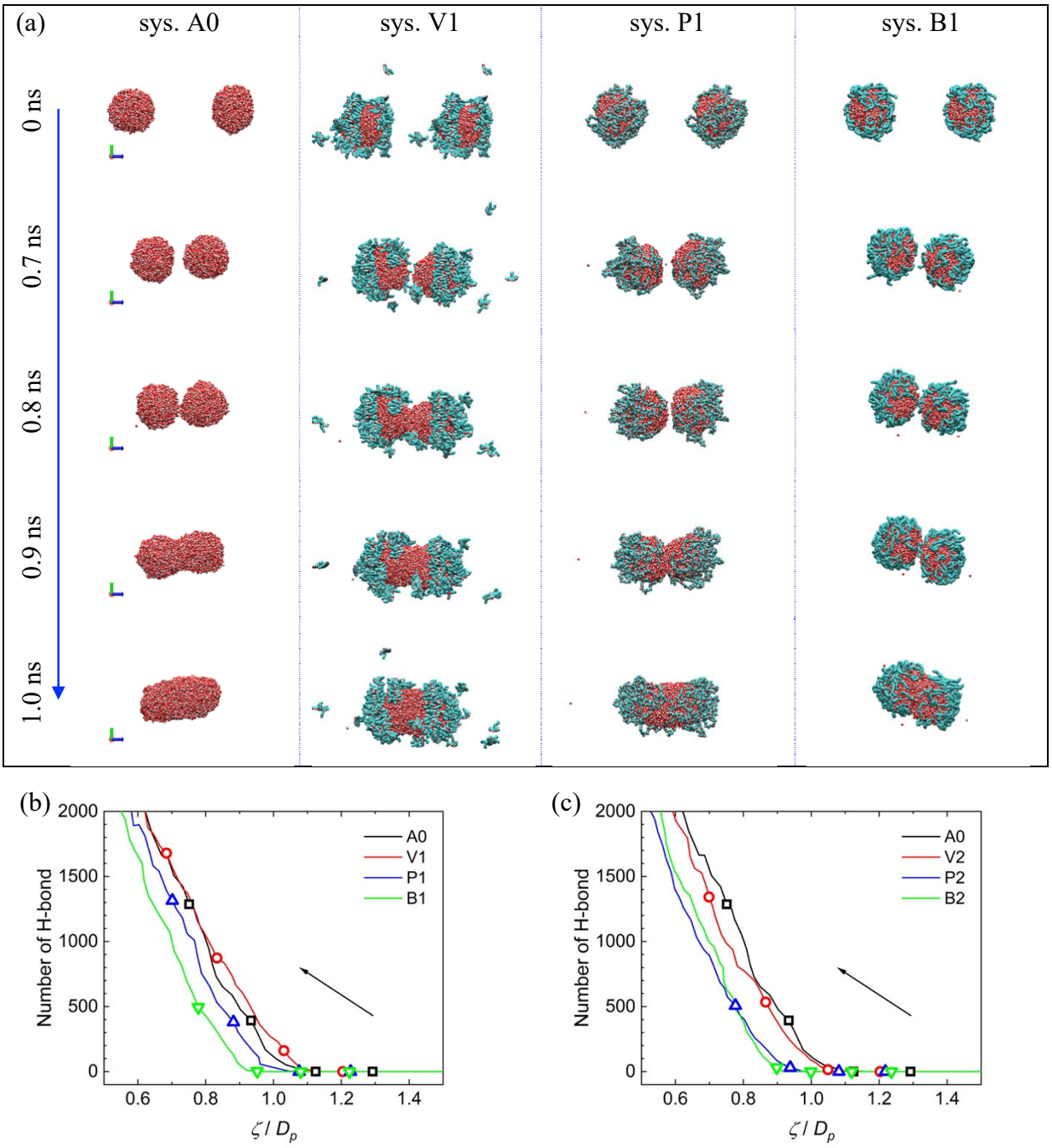

Figure 4. (a) Snapshots of the droplets at 0 ns, 0.7 ns, 0.8 ns, 0.9 ns, and 1.0 ns during SMD for sys. A0, V1, P1 and B1 (from left to right). Atoms are shown as van der Waals spheres, oxygen:

red; hydrogen: grey; carbon: cyan; toluene molecules eliminated for clarity. Corresponding snapshots for sys. V2, P2 and B2 are in SI section SI4. Number of hydrogen bonds vs. the COM separation (normalized by diameter of water droplet) during SMD for (b) sys. V1, P1, B1; (c) sys. V2, P2, B2. (sys. A0 is shown as reference; data points at time = 0.7, 0.8, 0.9, 1.0 ns are highlighted; arrows show the direction of time evolution.)

3.3 Potential of mean force calculated in simulations.

PMF (ΔG) was plotted against the reaction coordinates ζ (normalized by D_p) in Fig. 5a. The details of umbrella sampling were shown in SI section SI2. The range of reaction coordinate was selected to ensure sampling from the largest separation $\zeta / D_p \sim 2.25$-2.27 to the point after the coalescence occurred. The largest separation in each system was used as the reference where the PMF was set to zero. From the largest separation, PMF for sys. A0 slight decreased until $\zeta / D_p \sim 1.2$ and then drastically decreased. For sys. V1, the PMF increased to the maximum of $\Delta G_{max} = 23.0$ kcal/mol at $\zeta / D_p \sim 1.2$, followed by a rapid drop. The positive and increasing value of ΔG as the droplets approached each other (up to $\zeta / D_p \sim 1.2$) indicated repulsive interaction, and ΔG_{max} represented the energy barrier for droplet coalescence. Similar trend was observed in the PMF for sys. P1 and B1, and ΔG_{max} in these two systems were comparable to that in sys. V1. suggesting similar energy barrier caused by the three adsorbates. The difference among the three systems lied in the reaction coordinate at which ΔG_{max} occurred, which was $\zeta / D_p = 1.13$ in sys. P1 and $\zeta / D_p \sim 1.10$ in sys. B1.

In Fig. 5b, the mean force (F) between the two water droplets was calculated from the negative derivative of the PMF as: [50]

$$F(\zeta) = -\frac{\partial \Delta G}{\partial \zeta} \quad (1)$$

Without adsorbates (sys. A0), the interaction between the water droplets was negligible (F close to zero) when $\zeta / D_p > 1.2$ but became attractive (negative F) as coalescence started. For the systems with adsorbates, F underwent three stages as the droplets approached each other. In the first stage where $\zeta/D_p >\sim 2.0$, F was positive (*i.e.*, repulsive) and did not change significantly with the reaction coordinate. The repulsion was stronger in sys. V1 than in sys. P1 and B1. In the second stage ($\zeta_T/D_p < \zeta/D_p < 2.0$), F in each system increased as ζ / D_p decreased, until the maximum (F_{max}) was reached at a transition point $\zeta = \zeta_T$. F_{max} was similar for sys. V1, P1, B1, being 37 pN, 35 pN and 29 pN, respectively. The transition points ζ_T/D_p were also close: 1.48, 1.45 and 1.44 for the three systems. After the transition point, F started to decrease due to the attraction between water droplets and the formation of H-bonds as shown in Fig. 5b.

In Fig. 5a, similar trend was observed in the PMF curves for sys. V2, P2 or B2. The energy barrier for droplet coalescence was much higher for systems with more adsorbates (sys. V2, P2 or B2) than their counterparts that had less adsorbates (sys. V1, P1, or B1). Comparing different adsorbates, ΔG_{max} were ranked as sys. B2 > sys. V2 > sys. P2. As shown in Fig. 3b, the mean force F for sys. V2, P2 and B2 could also be distinguished in three stages, as was discussed for sys. V1, P1 and B2. In stage 1, F was again higher in sys. V2 than in sys. P2 or B2. However, in stage 2, F_{max} was quite different among the three systems and followed the same ranking for ΔG_{max}: sys. B2 > sys. V2 > sys. P2. The transition point ζ_T/D_p in sys. V2, P2 and B2 was 1.42, 1.44 and 1.16 respectively, at which F started to decrease.

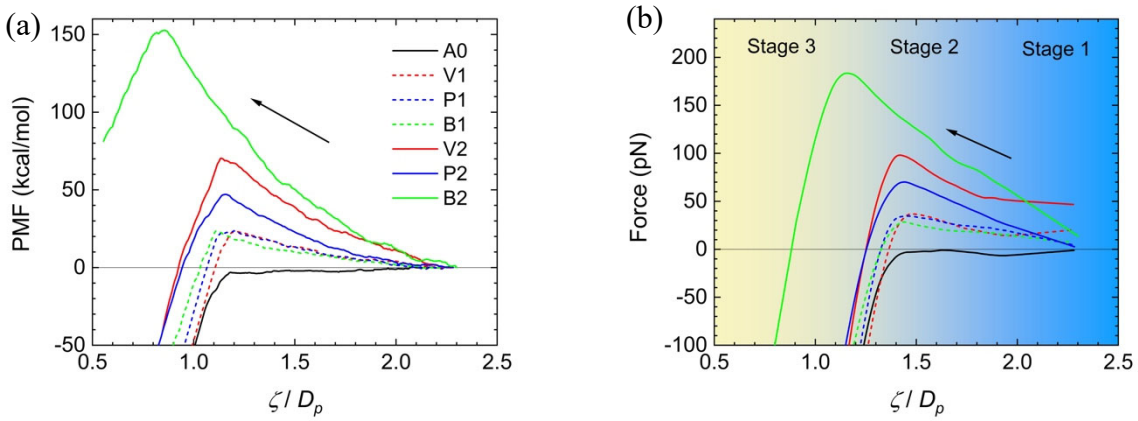

Figure 5. (a) PMF (ΔG) and (b) mean force (F) between two water droplets as they approached each other (direction indicated by arrows).

From the simulations, the mechanism of adsorbate-stabilized water droplet coalescence is summarized as follows.

Stage 1: At large COM separation ($\zeta/D_p > 2.0$), water droplets were under influence of weak repulsive force, indicated by the positive mean force F in Fig. 5b. The repulsion in systems containing VO-79 was stronger than that in systems containing $PEO_5PPO_{10}PEO_5$ or Brij-93, when comparing sys. V1 to P1 and B1, and sys. V2 to P2 and B2. One plausible explanation is that some VO-79 molecules were dispersed in the toluene phase and interfered with the approaching of water droplets. Thus, the repulsive force in this stage might be attributed to the hinderance from dispersed molecules in the toluene phase.

Stage 2: When $\zeta_T/D_p < \zeta/D_p < 2.0$, steric repulsion between the adsorbate films hindered droplet coalescence and the repulsion became stronger as the droplets became closer. Compared with the more hydrophilic groups (g1), the more hydrophobic groups (g2) in the adsorbates were located farther from the droplet surface (Fig. 3c and 3e). With water droplets approaching, the hydrophobic groups from different droplets came to contact first. At the same time, the steric repulsion pushed

the adsorbate molecules away from the contact zone and drove them to redistribute on the droplet surface (Fig. 4a and SI section SI4). If the droplet surfaces were only partially covered (sys. V1, P1, B1), there was sufficient room for adsorbate redistribution, leaving the contact zone exposed (Fig. 4a). The attractive interaction between water molecules reduced the mean force F to zero at the transition point. Similar energy barrier (ΔG_{max}) and maximum force (F_{max}) was observed in sys. V1, P1 and B1 (Fig. 5a-b), which might be attributed to the similar surface coverage fraction of the adsorbates. For systems with higher surface coverage (sys. V2, P2, B2), the majority of the droplet surface was covered by the adsorbates (Fig. 3a). Consequently, the repulsive force was stronger in sys. V2, P2, B2 compared with sys. V1, P1, B1, respectively. However, there was still a limited surface for the adsorbates to redistribute. As shown in Fig. 5b, sys. B2 had stronger repulsive force than sys. V2 and P2, probably due to the larger surface coverage in sys. B2 and less adsorbates drainage between the water droplets. Additionally, the adsorbate film in sys. B2 was thinner and the hydrophobic groups were located closer to the droplets as compared to sys. V2 and P2 (SI section SI3). Thus, it was more difficult for Brij-93 to redistribute (SI section SI4), resulting in higher F_{max} in sys. B2. Sys. P2 had higher surface coverage but lower F_{max} than sys. V2. As shown in Fig. 3e and SI section SI4, the polymer chains of $PEO_5PPO_{10}PEO_5$ formed a loosely structured film with the hydrophilic parts anchored at the droplet surface and hydrophobic parts extending into the toluene phase. Because of this loose structure, the polymeric chains were able to redistribute more easily on the droplet surface than VO-79 molecules, which contributed to the lower F_{max} in sys. P2.

Stage 3: In the final stage of coalescence where $\zeta/D_p < \zeta_T/D_p$, the exposed water molecules from the two droplets interacted and formed H-bonds. As shown in Fig. 4b-c, the number of H-bonds between the droplets drastically increased after their merging started. Strong H-bonds between

water molecules counteracted with the steric repulsion between adsorbates, which led to decrease in the mean force (increasing attraction). Also, the adsorbate molecules on different water droplets began to associate (SI section SI4), which further facilitated the coalescence.

In stages 1 and 2, ΔG increased with decreasing COM distance, indicating that coalescence was energetically unfavorable, and the water droplets were stabilized by the adsorbates. After overcoming the energy barriers in stage 3, the formation of H-bonds between water molecules and association of adsorbate molecules caused spontaneous coalescence as ΔG decreased from its peak value.

3.4 Interaction force measured by drop probe AFM.

The AFM force results for two water droplets (of similar radius 120~130 μm) in bare toluene and in solutions of different adsorbates are shown in Fig. 2b and Fig. 6a-f, respectively. In Fig. 2b, a weak hydrodynamic repulsion was detected when two water droplets approached each other in bare toluene, followed by jumping into contact and drop coalescence. The Hamaker constant between water surfaces in toluene is calculated to be 9.72×10^{-21} J, suggesting that the van der Waals interaction was strongly attractive which induced the droplet coalescence. The interaction forces between two water droplets in 5 and 1000 ppm VO-79 solutions are shown in Fig. 6a-b, respectively. Jump-in behaviors were observed after the repulsive force reached ~0.55 and ~0.62 nN for the two cases. Compared with the weak repulsion detected between two water droplets in Fig. 2b, the enhanced repulsion in Fig. 6a-b was mainly because of the steric effect from VO-79 molecules adsorbed on the water/toluene interfaces and the interference from dispersed VO-79. Nevertheless, the van der Waals attraction was sufficient to overcome the repulsion and drive the two water droplets to jump into contact leading to coalescence. The interfacial tension (IFT) results (SI section SI5) showed that the IFT of water/toluene interface deceased more at 1000 ppm VO-

79 than at 5 ppm VO-79, indicating that more VO-79 molecules were adsorbed at the water/toluene interface with higher VO-79 concentration. These IFT results were consistent with the slightly higher repulsion measured in Fig. 6b as compared in Fig. 6a. Similar results were obtained in Fig. 6c-d for the interaction forces between two water droplets in 5 and 1000 ppm Brij-93-in-toluene solutions, respectively. The repulsive force before jump-in reached 0.45 and 0.74 nN for 5 and 1000 ppm Brij-93, respectively. Fig. 6e-f show the force profiles measured between two water droplets in 0.1 and 5 ppm Pluronic P123-in-toluene solutions, respectively. For the 0.1 ppm case, jump-in behavior was observed after a repulsion of 0.39 nN was overcome. While under 5 ppm Pluronic P123, a small jump-in behavior was detected when the repulsion reached 0.36 nN. The interaction force then turned back to repulsion and reached the maximum of ~5 nN when the two water droplets were further compressed. During retraction, the upper water droplet detached from the lower one with a noticeable "stretching" and "jump-out" behavior. The adhesion between the two droplets reached as high as 12 nN before "jump-out". The IFT results (SI section SI5) showed that Pluronic P123 could adsorb to the water/toluene interface to lower the IFT, and the interfacial polymer chains could act as additional protective barrier to prevent the coalescence of the two droplets. The "stretching" and adhesion detected during retraction was most likely because of the interdigitation and hydrogen bonding interactions of the Pluronic P123 segments formed under compression.

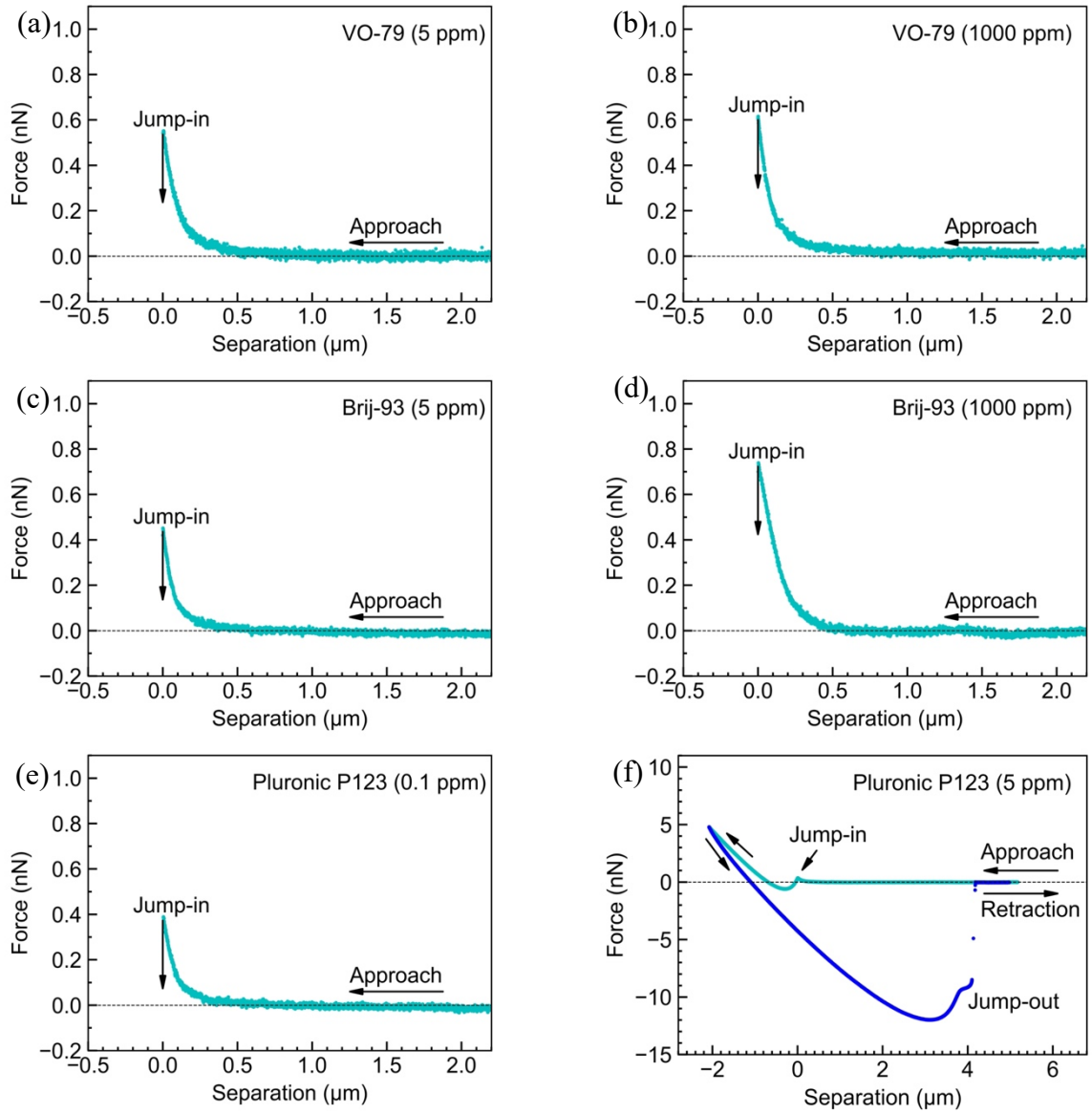

Figure 6. Interaction force profiles measured between two water droplets in toluene solutions with different adsorbates: (a) 5 ppm VO-79, (b) 1000 ppm VO-79, (c) 5 ppm Brij-93, (d) 1000 ppm Brij-93, (e) 0.1 ppm Pluronic P123, and (f) 5 ppm Pluronic P123. (Water droplet radius: 120~130 μm. Arrows indicate the movement of the water droplet on the cantilever.)

3.5 Implications.

As observed in MD simulations, interfacial-active materials adsorbed and formed barrier films at the surface of water droplets in toluene. To achieve similar surface coverage, as shown in Table 1 and SI section SI1, the mass concentration of VO-79 in sys. V1 had to be much higher than $PEO_5PPO_{10}PEO_5$ in sys. P1 or Brij-93 in sys. B1. With more adsorbates, the surface coverage by VO-79 (in sys. V2) was lower than the surface coverage by $PEO_5PPO_{10}PEO_5$ (in sys. P2) or Brij-93 (in sys. B2), even though the mass concentration of VO-79 was twice that of $PEO_5PPO_{10}PEO_5$ or Brij-93. The more difficulty of covering the water droplet with VO-79 than with surfactants ($PEO_5PPO_{10}PEO_5$ and Brij-93) was attributed to the following reasons. Firstly, VO-79 molecules were adsorbed mainly through the interaction between the PA cores in VO-79 and the water molecules (Fig. 3c and 3e). The atoms in the PA cores were located farther from the droplet surface than the hydrophilic groups in $PEO_5PPO_{10}PEO_5$ and Brij-93, which indicates that the PA cores were almost perpendicular to the surface, as suggested by the previous study[24] and shown in SI section SI6. In addition, PA cores from different VO-79 molecules formed stacking through π–π interactions[23] as observed in Fig. 3a. Such configuration tends to provide a poorer surface coverage than the one in which the PA cores are parallel to the surface. The hydrophilic chains in $PEO_5PPO_{10}PEO_5$ and Brij-93 were more closely adsorbed (Fig. 3c and 3e) which facilitated coverage of the droplet surface. Secondly, PACs had high solubility in aromatic solvent (*i.e.* toluene),[24] thus, the VO-79 molecules were partially adsorbed and some remained dispersed in bulk toluene (Fig. 3a and 4a). Experimentally (SI section SI5), the IFT at water/toluene interface was highest for system with 5 ppm VO-79, slightly lower in system with 5 ppm of Brij-93, and significantly low in system with 5 ppm of Pluronic P123. This was consistent with the simulation results that VO-79 molecules were more difficult to adsorb at the water/toluene interface. Though less surface-active than the two surfactants, VO-79 molecules were adsorbed at the droplet surface

and formed patchy and bulky film as observed in simulations. The interfacially adsorbed VO-79 sterically hindered water droplet coalescence, confirmed by both simulations (Fig. 5b) and AFM measurements (Fig. 6a-b), and consistent with the work of Shi *et al.*'s.[16] Also, the simulations (Fig. 5b) suggested that the dispersed VO-79 molecules contributed to the long-range stability of water droplets, as hypothesized by Jian *et al.*[51]

Comparing the two surfactants in MD simulations, the hydrophilic groups in $PEO_5PPO_{10}PEO_5$ and Brij-93 were adsorbed at a similar distance from the COM of the droplet, while the hydrophobic groups in $PEO_5PPO_{10}PEO_5$ were located farther than the hydrophobic groups in Brij-93 (Fig. 3c and 3e). The $PEO_5PPO_{10}PEO_5$ film was therefore less compact than the Brij-93 film on the droplet surface, compromising the surface coverage, as shown in SI section SI6. This can be seen from Table 1 where a higher mass concentration of $PEO_5PPO_{10}PEO_5$ in sys. P1 was needed to achieve a surface coverage comparable to sys. B1, and at a similar mass concentration, surface coverage in sys. P2 was lower than that in sys. B2. As shown in SI section SI5, the IFT reduction at water/toluene interface was similar for 0.1 ppm Pluronic P123 and 1000 ppm Brij-93. As Jian *et al.*[49] proposed, the reduction of IFT at water/oil interface was governed by the surface concentration and not the bulk concentration. Pluronic P123 at 0.1 ppm and Brij-93 at 1000 ppm, although hugely different in bulk concentration, might result in similar surface coverage at the water/toluene interface.

There are a few differences between the setups in simulations and in experiments. Partial surface coverage (46%-47%) on the water droplets was simulated in MD (sys. V1, P1, B1), while it could not be so-well controlled in the experiments. Also, the water droplets had nanometer size in simulations and micrometer size in AFM measurements, which can result in greater surface effect in the simulations. Because of these differences, the interaction forces from MD simulations

and AFM measurements were compared qualitatively instead of quantitatively. For example, from MD simulations (Fig. 5b), the interaction force between water droplets increased as the concentration of adsorbates and the droplet surface coverage increased. It was consistent with the AFM measurements (Fig. 6a-d) where the critical force which needed to be overcome before jump-in was higher for system with higher concentration of VO-79 or Brij-93. For Pluronic P123, similar jump-in phenomenon was only observed at the concentration of 0.1 ppm (Fig. 6e). IFT results (SI section SI5) suggested that the surface adsorption of 0.1 ppm Pluronic P123 was comparable to that of 1000 ppm Brij-93 and more significant than that of 1000 ppm VO-79. The critical force before jump-in was lower for 0.1 ppm Pluronic P123 compared with VO-79 and Brij-93 at both concentrations (5 ppm and 1000 ppm). This result was consistent with the MD results that the maximum repulsion F_{max} was lower for sys. P2 ($PEO_5PPO_{10}PEO_5$) than that for sys. V2 (VO-79) and sys. B2 (Brij-93). Among the AFM results, the maximum repulsive force before jump-in was highest for water droplets in 1000 ppm Brij-93-in-toluene solution, which was in agreement with the MD simulations where sys. B2 had the highest F_{max}. Although there have been reports that the dynamic IFT of a droplet can be size-dependent, the diffusion of surface-active molecules from the bulk to the interface played important roles in causing such differences. By applying a different bulk concentration in the simulations to effectively "expedite" the diffusion, we might have reached similar surface coverage at water/toluene interface as compared to experiments, which led to the good qualitative comparison.

PEO-PPO-PEO copolymers have been frequently used as demulsifiers to destabilize water-in-oil emulsions which were stabilized by surface-active components in oil, such as PACs.[52,53] The copolymers had higher affinity at the interface than PACs (SI section SI5), tended to adsorb at the water/oil interface and replace the PACs. Depending on the concentration of copolymers, the

demulsification mechanisms could be different. In the simulations, there were no (sys. P1) or only a few (sys. P2) dispersed copolymers in bulk toluene, and the interface could be considered undersaturated. In this case, the steric repulsion caused redistribution of the loosely structured copolymers at the interface (discussed in Fig. 5a-5b), which rendered lower repulsion between water droplets than the systems with PACs or Brij-93. The destabilization of water droplets in the case of low copolymer concentration was hence attributed to the lowering of repulsive force between water droplets by adding the copolymers as compared to the cases with PACs or Brij-93. On the other hand, if the water/oil interface was saturated by adsorbed copolymers, as shown in the AFM result for 5 ppm Pluronic P123 (Fig. 6f), the excessive copolymers could lead to stronger steric repulsion during approaching and form bridges between the two water droplets during separation. This result in turn led to adhesion between the two droplets which prevented their separation (Fig. 6f), providing another way to collect water-in-oil emulsion droplets and allow water/oil separation. This hypothesis could be confirmed by the simulation studies with increasing the concentration of copolymers. For future perspectives, the simulation method used in this work could be extended to similar systems to address the effect of concentration of adsorbates.

Another demulsifier,[27,28] Brij-93, also had higher affinity at the water/toluene interface compared with VO-79. During the demulsification, Brij-93 was shown to be able to replace the VO-79 at the interface and form a film closer to the water phase than VO-79.[31] Previous study simulated the water droplets stabilized by nanoparticles and stated that the water droplets were compressed prior the merging, where the deformation was more significant when there were more adsorbed nanoparticles.[54] As shown in SI section SI4, the water droplets was compressed during the coalescence and the deformation was more significant in sys. B2 with high concentration of Brij-93 compared with sys. B1 with low concentration of Brij-93. The surfactants used in this work

was not as rigid as the nanoparticles, however, the mobility of surfactant was compromised when the surface coverage was high in sys. B2. Coalescence of water droplets was observed in AFM measurements with both low and high concentrations of Brij-93. While the force right before jump-in was lower for Brij-93 than for VO-79 at 5 ppm concentration, at the concentration of 1000 ppm the force was higher for Brij-93 (Fig. 6b and 6d). Consistently in the simulations, at similar and high surface coverage (simulated as sys. V2 and B2), Brij-93 resulted in higher repulsive force during the coalescence (Fig. 5b). The results suggest that in order to promote water droplet coalescence, the dosage of Brij-93 needs to be properly modulated so that there are sufficient Brij-93 molecules to replace PACs from the interface while not too many to impose high repulsive (steric) forces.

4. CONCLUSIONS

MD simulations were performed on water droplets in toluene solutions with the presence of three types of adsorbates, a polycyclic aromatic compound (VO-79) and two non-ionic surfactants (PEO-PPO-PEO triblock copolymer; Brij-93). Potential of mean force during the coalescence of water-in-oil emulsion droplets was calculated, and the interaction forces were compared with experimental measurements using the drop probe AFM technique. Three stages of droplets coalescence were identified from the simulations. Dispersed VO-79 contributed to the strongest repulsion between the droplets. As the two droplets approached each other, the repulsion between them became stronger due to the increased steric repulsion between the adsorbate films. Meanwhile, the steric repulsion induced redistribution of adsorbate molecules on the droplet surface, leaving part of the surfaces uncovered and facing each other. The exposed water molecules from the two droplets interacted by forming H-bonds. Additionally, the adsorbates became interconnected on the surface of merged water droplet, counteracting the steric repulsion and

accelerating coalescence. Among the adsorbates, PEO-PPO-PEO copolymer formed a loose structure at the droplet surface and could redistribute more easily than VO-79 or Brij-93, which contributed to the lowest repulsion for droplet coalescence.

For VO-79 and Brij-93, the repulsion for droplet coalescence was found to increase with the concentration of adsorbates from both MD simulations and AFM force measurements. IFT and AFM force experiments suggested that, compared with VO-79, low concentration of PEO-PPO-PEO copolymer had high affinity at the water/toluene interface and lower repulsion between water droplets, which could facilitate the coalescence of VO-79 stabilized water droplets. However, when a high concentration of PEO-PPO-PEO copolymer was added in experiments, the adsorbed copolymer chains at the oil/water interface could lead to steric repulsion and prevent the drop coalescence. This study unravelled the interaction between water-in-oil emulsion droplets by correlating the results from MD simulations and AFM force measurements, and the methodologies could be extended to similar systems containing water droplets and surface-active molecules.

Acknowledgment

The authors gratefully acknowledge the computing resources and technical support from the Western Canada Research Grid (WestGrid), and the financial support from the Natural Sciences and Engineering Research Council of Canada (NSERC), Syncrude Canada Ltd., Suncor Energy, Canadian Natural Resources Limited, ChampionX, and the Future Energy Systems under the Canada First Research Excellence Fund.

Supporting information

Surface coverage fraction (SI1); Details of umbrella sampling (SI2); Location and width of RDF peaks (SI3); Additional snapshot during SMD (SI4); Interfacial tension measurements (SI5); Snapshots of final configurations for systems with a single adsorbate (SI6).

REFERENCES

(1) Shimizu, R.; Tanaka, H. A Novel Coarsening Mechanism of Droplets in Immiscible Fluid Mixtures. *Nat. Commun.* **2015**, *6*, 7407.

(2) Pawar, A. B.; Caggioni, M.; Ergun, R.; Hartel, R. W.; Spicer, P. T. Arrested Coalescence in Pickering Emulsions. *Soft Matter* **2011**, *7*, 7710.

(3) Fan, H.; Striolo, A. Mechanistic Study of Droplets Coalescence in Pickering Emulsions. *Soft Matter* **2012**, *8*, 9533.

(4) Factorovich, M. H.; Molinero, V.; Scherlis, D. A. Vapor Pressure of Water Nanodroplets. *J. Am. Chem. Soc.* **2014**, *136*, 4508–4514.

(5) Kamp, J.; Villwock, J.; Kraume, M. Drop Coalescence in Technical Liquid/Liquid Applications: A Review on Experimental Techniques and Modeling Approaches. *Rev. Chem. Eng.* **2017**, *33*, 1–47.

(6) Lee, D. J.; Kim, H. M.; Song, Y. S.; Youn, J. R. Water Droplet Bouncing and Superhydrophobicity Induced by Multiscale Hierarchical Nanostructures. *ACS Nano* **2012**, *6*, 7656–7664.

(7) Liao, M.-L.; Ju, S.-P.; Yang, S.-H. Coalescence Behavior of Water Nanoclusters: Temperature and Size Effects. *J. Phys. Chem. C* **2007**, *111*, 6927–6932.

(8) Perumanath, S.; Borg, M. K.; Chubynsky, M. V.; Sprittles, J. E.; Reese, J. M. Droplet Coalescence Is Initiated by Thermal Motion. *Phys. Rev. Lett.* **2019**, *122*, 104501.

(9) Yan, X.; Zhang, L.; Sett, S.; Feng, L.; Zhao, C.; Huang, Z.; Vahabi, H.; Kota, A. K.; Chen, F.; Miljkovic, N. Droplet Jumping: Effects of Droplet Size, Surface Structure, Pinning, and Liquid Properties. *ACS Nano* **2019**, *13*, 1309–1323.

(10) Zhang, L.; Xie, L.; Cui, X.; Chen, J.; Zeng, H. Intermolecular and Surface Forces at Solid/Oil/Water/Gas Interfaces in Petroleum Production. *J. Colloid Interface Sci.* **2019**, *537*, 505–519.

(11) Qiu, Y.; Molinero, V. Morphology of Liquid–Liquid Phase Separated Aerosols. *J. Am. Chem. Soc.* **2015**, *137*, 10642–10651.

(12) Xie, L.; Shi, C.; Cui, X.; Zeng, H. Surface Forces and Interaction Mechanisms of Emulsion Drops and Gas Bubbles in Complex Fluids. *Langmuir* **2017**, *33*, 3911–3925.

(13) Zhang, S.; Zhang, L.; Lu, X.; Shi, C.; Tang, T.; Wang, X.; Huang, Q.; Zeng, H. Adsorption Kinetics of Asphaltenes at Oil/Water Interface: Effects of Concentration and Temperature. *Fuel* **2018**, *212*, 387–394.

(14) Chiu, Y.-L.; Chan, H. F.; Phua, K. K. L.; Zhang, Y.; Juul, S.; Knudsen, B. R.; Ho, Y.-P.; Leong, K. W. Synthesis of Fluorosurfactants for Emulsion-Based Biological Applications. *ACS Nano* **2014**, *8*, 3913–3920.

(15) Sicard, F.; Toro-Mendoza, J.; Striolo, A. Nanoparticles Actively Fragment Armored Droplets. *ACS Nano* **2019**, *13*, 9498–9503.

(16) Shi, C.; Zhang, L.; Xie, L.; Lu, X.; Liu, Q.; He, J.; Mantilla, C. A.; Van den berg, F. G. A.; Zeng, H. Surface Interaction of Water-in-Oil Emulsion Droplets with Interfacially Active Asphaltenes. *Langmuir* **2017**, *33*, 1265–1274.

(17) Pensini, E.; Harbottle, D.; Yang, F.; Tchoukov, P.; Li, Z.; Kailey, I.; Behles, J.; Masliyah, J.; Xu, Z. Demulsification Mechanism of Asphaltene-Stabilized Water-in-Oil Emulsions by a

Polymeric Ethylene Oxide–Propylene Oxide Demulsifier. *Energy Fuels* **2014**, *28*, 6760–6771.
(18) Chen, Y.; Shen, C.; Peterson, G. P. Hydrodynamics and Morphologies of Droplet Coalescence. *Ind. Eng. Chem. Res.* **2015**, *54*, 9257–9262.
(19) Dokter, A. M.; Woutersen, S.; Bakker, H. J. Inhomogeneous Dynamics in Confined Water Nanodroplets. *Proc. Natl. Acad. Sci.* **2006**, *103*, 15355–15358.
(20) Vaitheeswaran, S.; Thirumalai, D. Hydrophobic and Ionic Interactions in Nanosized Water Droplets. *J. Am. Chem. Soc.* **2006**, *128*, 13490–13496.
(21) Wang, B.-B.; Wang, X.-D.; Yan, W.-M.; Wang, T.-H. Molecular Dynamics Simulations on Coalescence and Non-Coalescence of Conducting Droplets. *Langmuir* **2015**, *31*, 7457–7462.
(22) Zhao, L.; Choi, P. Molecular Dynamics Simulation of the Coalescence of Nanometer-Sized Water Droplets in *n* -Heptane. *J. Chem. Phys.* **2004**, *120*, 1935–1942.
(23) Jian, C.; Zeng, H.; Liu, Q.; Tang, T. Probing the Adsorption of Polycyclic Aromatic Compounds onto Water Droplets Using Molecular Dynamics Simulations. *J. Phys. Chem. C* **2016**, *120*, 14170–14179.
(24) Jian, C.; Liu, Q.; Zeng, H.; Tang, T. Effect of Model Polycyclic Aromatic Compounds on the Coalescence of Water-in-Oil Emulsion Droplets. *J. Phys. Chem. C* **2017**, *121*, 10382–10391.
(25) Pak, C. Y.; Li, W.; Steve Tse, Y.-L. Free Energy and Dynamics of Water Droplet Coalescence. *J. Phys. Chem. C* **2018**, *122*, 22975–22984.
(26) Pak, C. Y.; Li, W.; Steve Tse, Y.-L. Free Energy and Dynamics of Organic-Coated Water Droplet Coalescence. *J. Phys. Chem. C* **2020**, *124*, 8749–8757.
(27) Pradilla, D.; Simon, S.; Sjöblom, J. Mixed Interfaces of Asphaltenes and Model Demulsifiers, Part II: Study of Desorption Mechanisms at Liquid/Liquid Interfaces. *Energy Fuels* **2015**, *29*, 5507–5518.
(28) Pradilla, D.; Simon, S.; Sjöblom, J. Mixed Interfaces of Asphaltenes and Model Demulsifiers Part I: Adsorption and Desorption of Single Components. *Colloids Surf. Physicochem. Eng. Asp.* **2015**, *466*, 45–56.
(29) Sun, X.; Zeng, H.; Tang, T. Molecular Simulation of Folding and Aggregation of Multi-Core Polycyclic Aromatic Compounds. *J. Mol. Liq.* **2020**, *310*, 113248.
(30) Lan, T.; Zeng, H.; Tang, T. Molecular Dynamics Study on the Mechanism of Graphene Oxide to Destabilize Oil/Water Emulsion. *J. Phys. Chem. C* **2019**, *123*, 22989–22999.
(31) Sun, X.; Zeng, H.; Tang, T. Effect of Non-Ionic Surfactants on the Adsorption of Polycyclic Aromatic Compounds at Water/Oil Interface: A Molecular Simulation Study. *J. Colloid Interface Sci.* **2021**, *586*, 766–777.
(32) Frisch, M. J.; Trucks, G. W.; Schlegel, H. B.; Scuseria, G. E.; Robb, M. A.; Cheeseman, J. R.; Scalmani, G.; Barone, V.; Petersson, G. A.; Nakatsuji, H., et al. *Gaussian 16 Rev. C.01*; Gaussian, Inc.: Wallingford, CT, 2016.
(33) Becke, A. D. A New Mixing of Hartree–Fock and Local Density-functional Theories. *J. Chem. Phys.* **1993**, *98*, 1372–1377.
(34) Breneman, C. M.; Wiberg, K. B. Determining Atom-Centered Monopoles from Molecular Electrostatic Potentials. The Need for High Sampling Density in Formamide Conformational Analysis. *J. Comput. Chem.* **1990**, *11*, 361–373.

(35) Malde, A. K.; Zuo, L.; Breeze, M.; Stroet, M.; Poger, D.; Nair, P. C.; Oostenbrink, C.; Mark, A. E. An Automated Force Field Topology Builder (ATB) and Repository: Version 1.0. *J. Chem. Theory Comput.* **2011**, *7*, 4026–4037.
(36) Schuler, L. D.; Daura, X.; Gunsteren, W. F. van. An Improved GROMOS96 Force Field for Aliphatic Hydrocarbons in the Condensed Phase. *J. Comput. Chem.* **2001**, *22*, 1205–1218.
(37) Spoel, D. V. D.; Lindahl, E.; Hess, B.; Groenhof, G.; Mark, A. E.; Berendsen, H. J. C. GROMACS: Fast, Flexible, and Free. *J. Comput. Chem.* **2005**, *26*, 1701–1718.
(38) Lindahl, E.; Hess, B.; van der Spoel, D. Gromacs 3.0: A Package for Molecular Simulation and Trajectory Analysis. *J. Mol. Model.* **2001**, *7*, 306–317.
(39) Berendsen, H. J. C.; van der Spoel, D.; van Drunen, R. Gromacs: A Message-Passing Parallel Molecular Dynamics Implementation. *Comput. Phys. Commun.* **1995**, *91*, 43–56.
(40) Oostenbrink, C.; Villa, A.; Mark, A. E.; Gunsteren, W. F. V. A Biomolecular Force Field Based on the Free Enthalpy of Hydration and Solvation: The Gromos Force-Field Parameter Sets 53a5 and 53a6. *J. Comput. Chem.* **2004**, *25*, 1656–1676.
(41) Saito, H.; Nagao, H.; Nishikawa, K.; Kinugawa, K. Molecular Collective Dynamics in Solid Para-Hydrogen and Ortho-Deuterium: The Parrinello–Rahman-Type Path Integral Centroid Molecular Dynamics Approach. *J. Chem. Phys.* **2003**, *119*, 953–963.
(42) Hess, B. P-LINCS: A Parallel Linear Constraint Solver for Molecular Simulation. *J. Chem. Theory Comput.* **2008**, *4*, 116–122.
(43) Essmann, U.; Perera, L.; Berkowitz, M. L.; Darden, T.; Lee, H.; Pedersen, L. G. A Smooth Particle Mesh Ewald Method. *J. Chem. Phys.* **1995**, *103*, 8577–8593.
(44) Sevick, E. M.; Monson, P. A.; Ottino, J. M. Monte Carlo Calculations of Cluster Statistics in Continuum Models of Composite Morphology. *J. Chem. Phys.* **1988**, *88*, 1198–1206.
(45) Lemkul, J. A.; Bevan, D. R. Assessing the Stability of Alzheimer's Amyloid Protofibrils Using Molecular Dynamics. *J. Phys. Chem. B* **2010**, *114*, 1652–1660.
(46) You, W.; Tang, Z.; Chang, C. A. Potential Mean Force from Umbrella Sampling Simulations: What Can We Learn and What Is Missed? *J. Chem. Theory Comput.* **2019**, *15*, 2433–2443.
(47) Hub, J. S.; de Groot, B. L.; van der Spoel, D. G_wham—A Free Weighted Histogram Analysis Implementation Including Robust Error and Autocorrelation Estimates. *J. Chem. Theory Comput.* **2010**, *6*, 3713–3720.
(48) Hutter, J. L.; Bechhoefer, J. Calibration of Atomic-force Microscope Tips. *Rev. Sci. Instrum.* **1993**, *64*, 1868–1873.
(49) Jian, C.; Poopari, M. R.; Liu, Q.; Zerpa, N.; Zeng, H.; Tang, T. Reduction of Water/Oil Interfacial Tension by Model Asphaltenes: The Governing Role of Surface Concentration. *J. Phys. Chem. B* **2016**, *120*, 5646–5654.
(50) Kopelevich, D. I. One-Dimensional Potential of Mean Force Underestimates Activation Barrier for Transport across Flexible Lipid Membranes. *J. Chem. Phys.* **2013**, *139*, 134906.
(51) Jian, C.; Liu, Q.; Zeng, H.; Tang, T. Effect of Model Polycyclic Aromatic Compounds on the Coalescence of Water-in-Oil Emulsion Droplets. *J. Phys. Chem. C* **2017**, *121*, 10382–10391.
(52) Le Follotec, A.; Pezron, I.; Noik, C.; Dalmazzone, C.; Metlas-Komunjer, L. Triblock Copolymers as Destabilizers of Water-in-Crude Oil Emulsions. *Colloids Surf. Physicochem. Eng. Asp.* **2010**, *365*, 162–170.

(53) Wang, D.; Yang, D.; Huang, C.; Huang, Y.; Yang, D.; Zhang, H.; Liu, Q.; Tang, T.; Gamal El-Din, M.; Kemppi, T.; et al. Stabilization Mechanism and Chemical Demulsification of Water-in-Oil and Oil-in-Water Emulsions in Petroleum Industry: A Review. *Fuel* **2021**, *286*, 119390.
(54) Sicard, F.; Striolo, A. Numerical Analysis of Pickering Emulsion Stability: Insights from ABMD Simulations. *Faraday Discuss.* **2016**, *191*, 287–304.

TOC Graphic

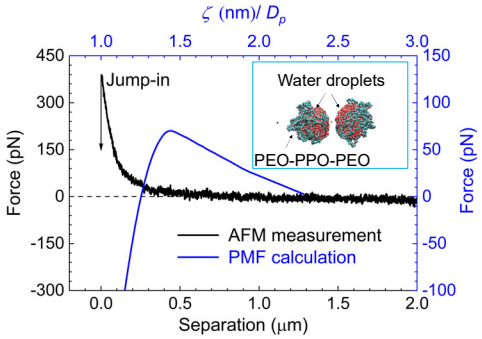
ζ (nm)/ D_p
1.0
1.5
2.0
2.5
3.0
450
300
150
0
-150
-300
150
100
50
0
-50
-100
Force (pN)
Force (pN)
Jump-in
Water droplets
PEO-PPO-PEO
AFM measurement
PMF calculation
0.0
0.5
1.0
1.5
2.0
Separation (μm)